SCIENTIFIC REPORTS

OPEN

SUBJECT AREAS:
CONDENSED-MATTER PHYSICS
THEORY AND COMPUTATION

Received
26 March 2014

Accepted
1 July 2014

Published
21 July 2014

Correspondence and requests for materials should be addressed to T.C. (cuitian@jlu.edu.cn)

Miscibility and ordered structures of MgO-ZnO alloys under high pressure

Fubo Tian, Defang Duan, Da Li, Changbo Chen, Xiaojing Sha, Zhonglong Zhao, Bingbing Liu & Tian Cui

State Key Laboratory of Superhard Materials, College of physics, Jilin University, Changchun 130012, P. R. China.

The $Mg_xZn_{1-x}O$ alloy system may provide an optically tunable family of wide band gap materials that can be used in various UV luminescences, absorption, lighting, and display applications. A systematic investigation of the MgO-ZnO system using *ab initio* evolutionary simulations shows that $Mg_xZn_{1-x}O$ alloys exist in ordered ground-state structures at pressures above about 6.5 GPa. Detailed enthalpy calculations for the most stable structures allowed us to construct the pressure-composition phase diagram. In the entire composition, no phase transition from wurzite to rock-salt takes place with increasing Mg content. We also found two different slops occur at near $x = 0.75$ of E_g-x curves for different pressures, and the band gaps of high pressure ground-state $Mg_xZn_{1-x}O$ alloys at the Mg concentration of $x > 0.75$ increase more rapidly than $x < 0.75$.

To realize high-performance ZnO-based optoelectronic devices, two important requirements are necessary: one is *p*-type doping of ZnO, and the other is modulation of the band gap (E_g)[1,2]. ZnO can alloy with MgO to form the ternary compound $Mg_xZn_{1-x}O$ to extend the energy band gap, and therefore the detection spectrum into the shorter wavelength region. While *p*-type doping of ZnO is studied intensively, the latter has been demonstrated by the development research on $Mg_xZn_{1-x}O$ allowing modulation of band gap in a wide range, from 3.34 to 7.8 eV[3]. Although the topic of ZnO has been extensively researched, less is known concerning the detailed structures of the $Mg_xZn_{1-x}O$ alloy system.

Fabrication and characterization of $Mg_xZn_{1-x}O$ alloy are important from the viewpoint of band gap modulation as well as of *p*–*n* junction. $Mg_xZn_{1-x}O$ thin films and nanostructures that include nanocrystals as well as core-shell structures have recently been studied with the objective of achieving a viable alloy family with tunable band gap and luminescence at the UV range[4–21]. Sans et al.[4] investigated the dependence of the phase transition on the hydrostatic pressure and found that the wurtzite to rock-salt transition pressure is observed to decrease from 9.5 ± 0.2 pure (ZnO) to 7.0 ± 0.2 GPa (for $x = 0.13$), with an almost linear dependence on the Mg content. Difficulties for the growth of high quality $Mg_xZn_{1-x}O$ films are partly from the fact that MgO (cubic) and ZnO (hexagonal) have different crystal structures at normal conditions.

In the last decade, there are numerous theoretical studies on the MgO-ZnO alloys[22–40]. Sanati *et al.*[22] showed that isostructural MgO-ZnO alloys are stable under certain conditions using the cluster expansion (CE) method, but they also concluded that if MgO and ZnO can adopt their own crystal structures (*B*1 and *B*4, respectively), the alloy is predicted to phase separate. This means that $Mg_xZn_{1-x}O$ alloys are not thermodynamically stable, consistent with a rather low observed solid solubility limit for Mg in ZnO. The cluster-expansion method was also used by Seko *et al.*[23] for investigating phase transitions, including vibrational effects through lattice dynamics calculations. Very recently, combining the CASP-CE with a systematic set of first-principles total energies, Liu *et al.*[24] exhaustively searched for the ground-state structures of MgO-ZnO alloys, and found a few structures as yet unreported. Several groups[25–29] reported their theoretical studies in which the random $Mg_xZn_{1-x}O$ alloy have been simulated using special quasirandom structures (SQS) approach[41,42]. There exist other theoretical studies[30–35], in which alloying of ZnO and MgO proceeds by substituting Mg atoms by Zn atoms in the cubic rock-salt structure or *vice versa* in the hexagonal wurtzite structure, and also exist several theoretical reports[36–38] on $MgZnO_2$ in various model systems. An extensive systematic study of structural properties of $Mg_xZn_{1-x}O$ was performed by Fan *et al.*[39] using a supercell approach within the local-density approximation. In another theoretical study[40], alloying of MgO and ZnO is described within coherent-potential approximation (CPA)[43].

Bulk and undoped ZnO prefers the hexagonal wurtzite (*B*4) structure under normal conditions and transforms into a cubic rocksalt (*B*1) structure at a pressure in the vicinity of 9 GPa reported by some experiments[44–46], while MgO adopts the cubic rocksalt structure up to the highest pressure of 227 GPa[47]. Generally, a large crystal structure difference between the wurtzite-hexagonal ZnO (*B*4) and the rock-salt-cubic MgO (*B*1) can cause

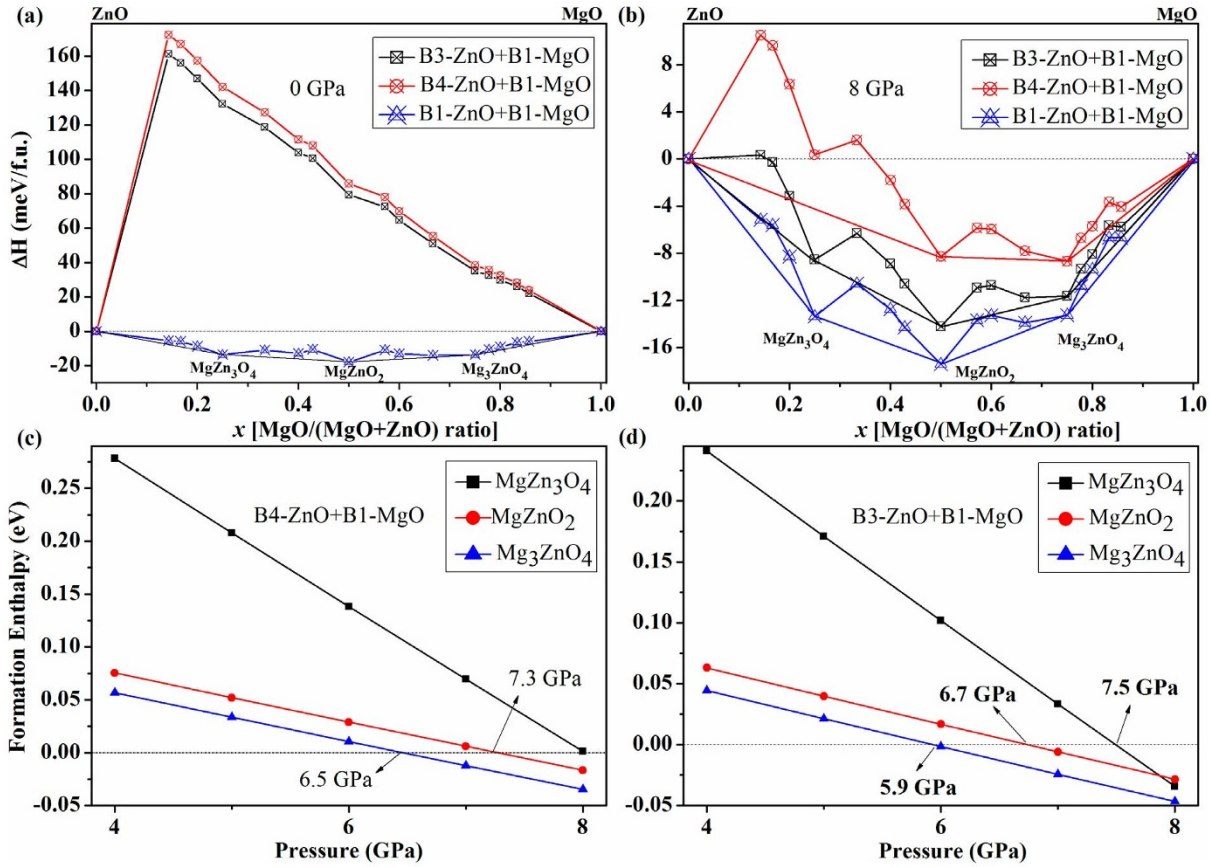

Figure 1 | **Thermal stability of MgO-ZnO alloys.** a,b Predicted formation enthalpy of MgO-ZnO alloys with respect to decomposition into B1-MgO and ZnO (B4, B3, or B1) at (a) 0 GPa and (b) 8 GPa. c,d Predicted formation enthalpy of $MgZn_3O_4$, $MgZnO_2$, and Mg_3ZnO_4 with respect to decomposition into B1-MgO and (c)B4-ZnO or (d) B3-ZnO below 8 GPa.

unstable phase mixing[6,48], as reported by Sanati *et al.*[22]. The same conclusions are made by Seko *et al.*[23] and Malashevich *et al.*[30], who both get that the formation energy of $Mg_xZn_{1-x}O$ is positive. Are there any stable structures of $Mg_xZn_{1-x}O$ alloy when ZnO and MgO adopt the same structure (*B*1) at pressures greater than 9 GPa? However, for the ordered structures of $Mg_xZn_{1-x}O$ under high pressure, few theoretical studies have been reported to the best of our knowledge. Therefore, a first-principles calculation is very interesting to investigate the high pressure stable structures of $Mg_xZn_{1-x}O$, because they are the basis of all properties in theoretical studies and can also provide valuable information for experimental synthesis.

Here, we investigate the possible stability of MgO-ZnO alloys under high pressure using the first-principles calculations, and the structures are obtained from a recently developed evolutionary algorithm for the prediction of crystal structures[49,50]. We also analyse the band gaps of these alloys.

Results

In this work, we report a few stable ground state structures of $Mg_xZn_{1-x}O$. The phase stabilities of MgO-ZnO systems are investigated by calculating the formation enthalpy of various $Mg_xZn_{1-x}O$ alloys at different pressures. The formation enthalpy of $Mg_xZn_{1-x}O$ is calculated by using fractional representation $Mg_xZn_{1-x}O$ ($0 \le x \le 1$) with respect to the decomposition into MgO and ZnO, as

$$\Delta H(Mg_xZn_{1-x}O) = H(Mg_xZn_{1-x}O) - [xH_{B1}(MgO) + (1-x)H_{B3,B4,B1}(ZnO)],$$

where the enthalpies H for $Mg_xZn_{1-x}O$ are obtained for the most stable structures as searched at the desired pressures. For MgO, the known structure *B*1 at our studied pressure is considered. For ZnO, transition from *B*4 to *B*1 takes place at 8.8 GPa as suggested by our enthalpy calculation (see Supplementary Fig. S1), which is in good consistency with the experimental findings $p_t \approx 8.7$ GPa[44], $p_t \approx 9.1$ GPa[45], or $p_t \approx 10$ GPa[46] and first-principles calculations $p_t = 9.3$ GPa[51]. It can also be seen that the B3 phase is slightly higher in energy than the B4 phase of ZnO. So, the enthalpies H for ZnO below 8.8 GPa, B4, B3 and B1 phases are all considered, for the reason of the lowest energy, lower energy and cubic structure, and B1-MgO-like structure, respectively, and above 8.8 GPa, only B1-ZnO is considered for the lowest energy and B1-MgO-like structure. The formation enthalpies of MgO-ZnO alloys under conditions of high pressure are depicted in Fig. 1 and Fig. 2. From Fig. 1 we noticed that $MgZn_3O_4$, $MgZnO_2$, and Mg_3ZnO_4 made from B1-MgO and B1-ZnO are thermodynamically stable at zero pressure because of their negative formation enthalpy, which is consistent with the results reported by Liu *et al.*[24] While in the case of B4-ZnO (or B3-ZnO) and B1-MgO, the formation enthalpies of all $Mg_xZn_{1-x}O$ alloys we got are positive below 6.5 GPa (or 5.9 GPa), indicating the tendency for segregation of the ZnO and MgO, in agreement with the calculated results at ambient pressure of previous theoretical studies[22,23,40].

Further detailed calculations above 8.8 GPa found a number of $Mg_xZn_{1-x}O$ stable against decomposition into the constituent oxides (B1-ZnO, B1-MgO, or $Mg_xZn_{1-x}O$). The formation enthalpies are shown in Fig. 2 for pressures of 10, 40, 60, and 80 GPa, and detailed enthalpy calculations for the most stable structures allowed us to construct the *P*-*x* phase diagram of the MgO-ZnO alloys (see Fig. 3). When the pressure reaches 10 GPa or higher, the formation enthalpies of all $Mg_xZn_{1-x}O$ alloys we predicted become negative. This is interesting trend for the number of $Mg_xZn_{1-x}O$ alloy to

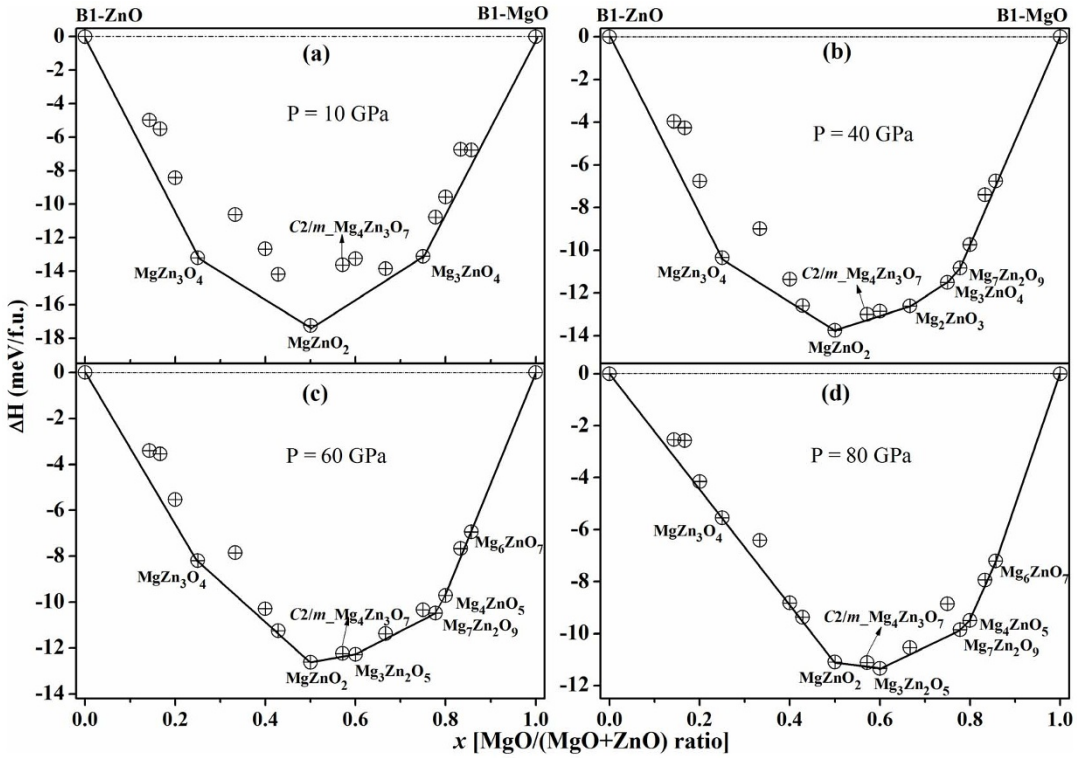

Figure 2 | **Thermal stability of MgO-ZnO alloys.** Predicted formation enthalpy of MgO-ZnO alloys with respect to decomposition into B1-MgO and B1-ZnO at (a) 10 GPa, (b) 40 GPa, (c) 60 GPa, and (d) 80 GPa, respectively.

increase with increasing pressure. In this direction, high pressure is obviously the right tool to widen the range of compositions in which the stable structures can be obtained. To the contrary, the structures of Mg_2ZnO_3 and Mg_3ZnO_4 become metastable when pressure is increased above about 50 GPa. This resulted in a confirmation of the following structures as DFT predicted ground states under different pressures: $MgZn_3O_4$ (*Pm*-3*m*, *I*4/*mmm*), $MgZnO_2$ (*P*4/*mmm*, $I4_1/amd$), $Mg_3Zn_2O_5$ (*C*2/*m*), Mg_2ZnO_3 (*Cmcm*), Mg_3ZnO_4 (*Pm*-3*m*, *I*4/*mmm*), Mg_4ZnO_5 (*I*4/*m*), $Mg_7Zn_2O_9$ (*C*2/*m*), and Mg_6ZnO_7 (*R*-3). For all the predicted structures as shown in Fig. 4 we computed phonon dispersions (see Supplementary Fig. S2) in the pressure range of 0–80 GPa, and found them to be dynamically stable.

As can be seen from Fig. 2, at 10 GPa, the energetically "deepest" structures occur at x = 0.25, x = 0.5 and x = 0.75, which have been extensively studied by many authors[22–26]. Two structures were found respectively at the three compositions under pressure bellow 80 GPa, and the enthalpies difference are depicted in Fig. 5. It should be pointed out that the enthalpy differences are only within a few meV/formula. At 6.5 (or 5.9 GPa for B3-ZnO considered) to

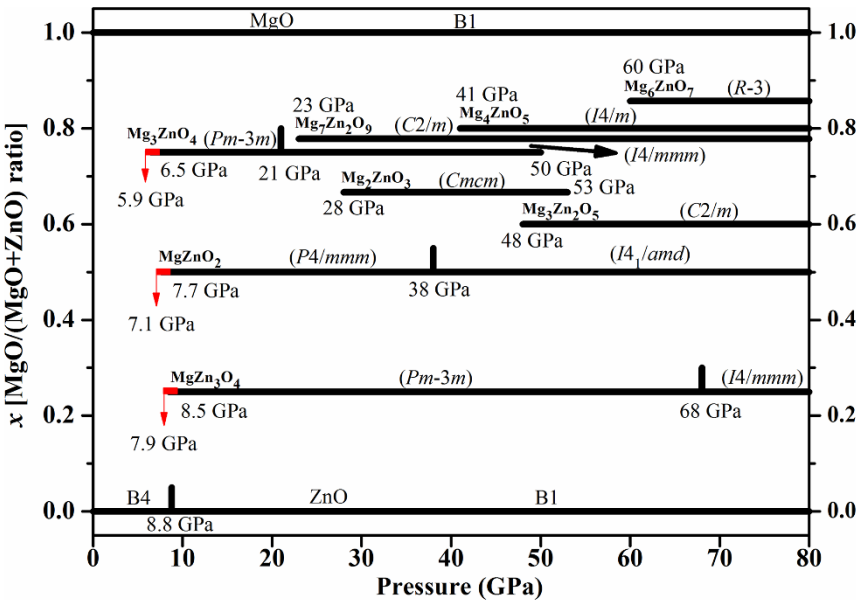

Figure 3 | **Pressure-composition phase diagram of the $Mg_xZn_{1-x}O$ alloys.** Red line represents the pressures at which $MgZn_3O_4$, $MgZnO_2$, and Mg_3ZnO_4 become stable against decomposition into B3-ZnO and other oxides ($Mg_xZn_{1-x}O$, or B1-MgO).

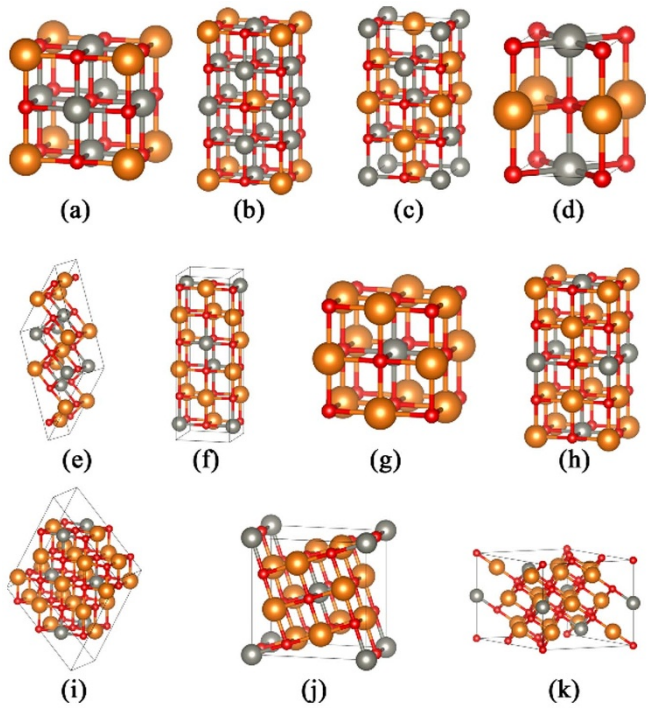

Figure 4 | Crystal structures of the predicted $Mg_xZn_{1-x}O$ alloys. (a) *Pm*-3*m*_$MgZn_3O_4$, (b) *I*4/*mmm*_$MgZn_3O_4$, (c) $I4_1/amd$_$MgZnO_2$, (d) *P*4/*mmm*_$MgZnO_2$, (e) C/*m*_$Mg_3Zn_2O_5$, (f) *Cmcm*_Mg_2ZnO_3, (g) *Pm*-3*m*_Mg_3ZnO_4, (h) *I*4/*mmm*_Mg_3ZnO_4, (i) *C*2/*m*_$Mg_7Zn_2O_9$, (j) *I*4/*m*_Mg_4ZnO_5, (k) *R*-3_Mg_6ZnO_7. The large orange, middle gray and small red spheres represent Mg, Zn and O atoms, respectively. For more structural details, see the Supplementary Table S1 online.

21 GPa, Mg_3ZnO_4 is stable in the *Pm*-3*m* structure ($L1_2$-type, as reported in Ref. 25), and then transforms into a tetragonal *I*4/*mmm* structure ($D0_{22}$-type), which is the same as that reported in Refs.[22,24]. For $MgZn_3O_4$, the cubic *Pm*-3*m* and tetragonal *I*4/*mmm* phases are found to be the most stable in pressure ranges of 8.5 (or 7.9 GPa for B3-ZnO considered)-68 and 68–80 GPa, respectively. The *Pm*-3*m* $MgZn_3O_4$ ($L1_2$-type) is the same as that reported in Refs[24,25]. $MgZnO_2$ is stable in the *P*4/*mmm* structure (same as that in Ref. 25) at 7.7 GPa (or 7.1 GPa for B3-ZnO considered), and transforms into a tetragonal $I4_1/amd$ structure (same as "40"-type reported in Ref.24) at 38 GPa, which is stable up to at least 80 GPa. Fig. 5(b) shows that both of the $MgZnO_2$ structures are more stable rather than in chalcopyrite structure[37,38]. It is emphasized that the structural researches of Refs[22,24,25] are all performed at atmospheric pressure.

Detailed calculations and analysis of the other structures under higher pressure are performed and show other five stable MgO-rich MgO-ZnO alloys made from isostructural components (*B*1-MgO and *B*1-ZnO): Mg_2ZnO_3 (Fig. 4(f); space group *Cmcm*), stable in a pressure range of 28–53 GPa; and $Mg_7Zn_2O_9$ (Fig. 4(i); space group *C*2/*m*), Mg_4ZnO_5 (Fig. 4(j); space group *I*4/*m*), $Mg_3Zn_2O_5$ (Fig. 4(e); space group *C*2/*m*), and Mg_6ZnO_7 (Fig. 4(k); space group *R*-3), which are stable above 23 GPa, 41 GPa, 48 GPa, and 60 GPa, respectively. Among the five phases of $Mg_xZn_{1-x}O$ alloy, the *C*2/*m* $Mg_7Zn_2O_9$ is the same as R1-$Mg_7Zn_2O_9$ (*C*2/*m*) reported in Ref.[24]. For the MgO-rich side of the phase diagram, we predict a stable hexagonal *R*-3 Mg_6ZnO_7, which confirms the possibility that $Mg_xZn_{1-x}O$ crystallizes in a hexagonal structure at high concentrations *x*, as recently reported by Shimada *et al.*[35]. This is a very interesting case due to the point that $Mg_xZn_{1-x}O$ alloy with high concentrations *x* have long been thought to adopt rocksalt (cubic) structures. Especially, the MgO-ZnO alloys more should be *B*1-like structure since both MgO and ZnO are stable in *B*1 phase above 8.8 GPa. In addition, our calculated formation enthalpy data of metastable *C*2/*m*-$Mg_4Zn_3O_7$ is slightly above the convex hull up to

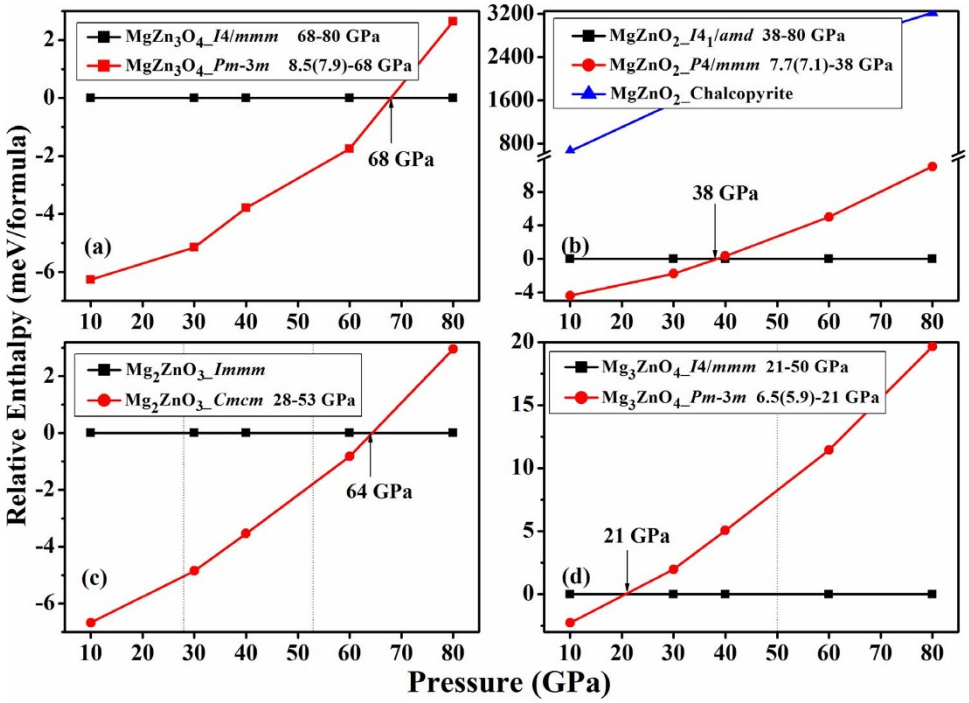

Figure 5 | Calculated enthalpies as the function of pressure. (a) Enthalpy curves (relative to *I*4/*mmm* phase) for *Pm*-3*m* $MgZn_3O_4$, (b) Enthalpy curves (relative to $I4_1/amd$ phase) for *P*4/*mmm* $MgZnO_2$, (c) Enthalpy curves (relative to *Immm* phase) for *Cmcm* Mg_2ZnO_3, and (d) Enthalpy curves (relative to *I*4/*mmm* phase) for *Pm*-3*m* Mg_3ZnO_4 by CASTEP code. The values in brackets represent the pressures at which $MgZn_3O_4$, $MgZnO_2$, and Mg_3ZnO_4 become stable against decomposition into B3-ZnO and other oxides ($Mg_xZn_{1-x}O$, or B1-MgO).

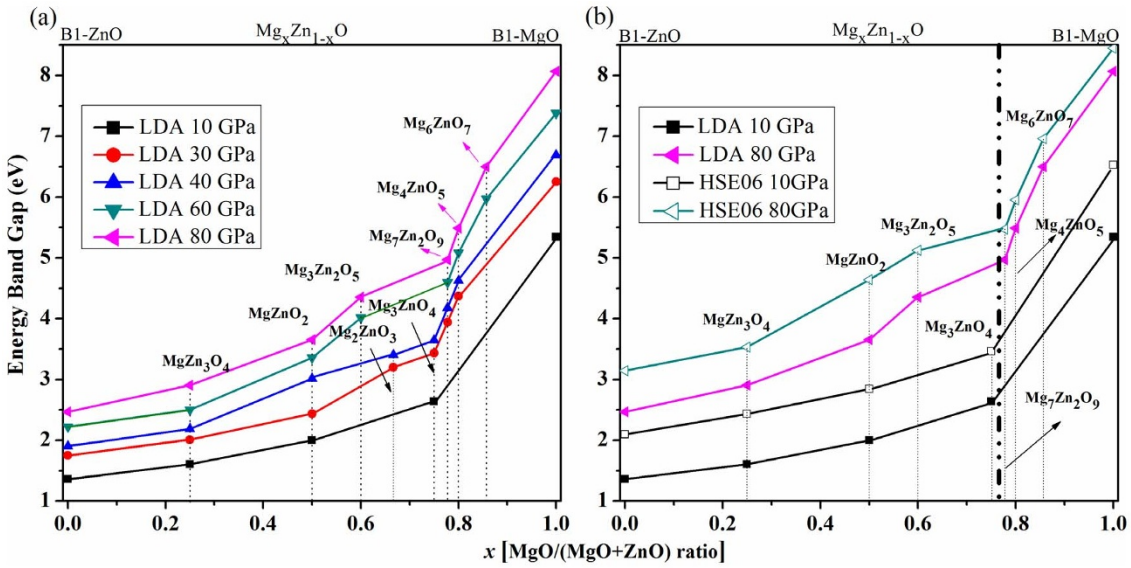

Figure 6 | Band-gap variation of $Mg_xZn_{1-x}O$ alloys as a function of MgO concentration at different pressures. (a) Calculated LDA band gaps, (b) Comparison of LDA band gaps with HSE06 values.

80 GPa, which is different from their report on R2-$Mg_4Zn_3O_7$ (*C*2/*m*) as one of ground-state structures[24].

Figure 6 illustrates the calculated band gaps as a function of Mg composition using the the local density approximation (LDA-CAPZ)[52,53] functional and screened hybrid functional of Heyd, Scuseria, and Ernzerhof (HSE06)[54,55] for the ground-state $Mg_xZn_{1-x}O$ structures under high pressure. From Fig. 6(a), it can be clearly seen that the gap increases with increase in the Mg content at the same pressure and increases with pressure increased at the same concentration. In addition, two different slops occur at about $x = 0.75$ of E_g-x curves for different pressures, which agrees with the findings reported in previous works[40,56–58], in which the change of slope near one composition value has been attributed to structural phase from wurtzite to cubic with Mg content increased. Our calculated results show that no phase transition from wurzite to cubic or vice versa takes place at the point where the slope changes, and we consider that the band gaps of $Mg_xZn_{1-x}O$ strongly dependent on the Mg content. The HSE06 functional results are depicted in Fig. 6(b), which show the same trend as the LDA values, with the difference of 0.5–1.0 eV higher value at the same pressure.

Discussion

We have performed a systematic theoretical investigation of the compositions and structures of the MgO-ZnO alloys and identified the stable ground-state structures as well as a number of metastable structures at 0–80 GPa over a wide range of Mg concentrations. Our results show that stable ordered ground-state $Mg_xZn_{1-x}O$ alloys only occur at high pressure. As well as recognizing the previous theoretically observations for the $MgZn_3O_4$ (*Pm*-3*m*), $MgZnO_2$ (*P*4/*mmm*, *I*4$_1$/*amd*), Mg_3ZnO_4 (*Pm*-3*m*, *I*4/*mmm*), and $Mg_7Zn_2O_9$ (*C*2/*m*) at atmospheric pressure as high pressure stable phases, the new stable alloys $MgZn_3O_4$ (*I*4/*mmm*), $Mg_3Zn_2O_5$ (*C*2/*m*), Mg_2ZnO_3 (*Cmcm*), Mg_4ZnO_5 (*I*4/*m*), and Mg_6ZnO_7 (*R*-3), have been predicted in the ground state under different pressure ranges. Among these structures, only Mg_6ZnO_7 with a high Mg content crystallizes in the hexagonal structure under high pressure, and for the entire alloy composition of $Mg_xZn_{1-x}O$, there is no phase transition from wurzite to cubic or vice versa takes place. Moreover, the band gaps of MgO-ZnO alloys with high MgO content increase more rapidly than low MgO content.

The high pressure ground-state and metastable structures are all metastable at ambient pressure and may be synthesized under certain conditions (e.g., at high temperature).

Methods

Crystal structure prediction. The ground state structures of $Mg_xZn_{1-x}O$ below 80 GPa are predicted by the *ab initio* evolutionary algorithm USPEX[49,50]. We have performed variable-composition simulation through the USPEX code in the range of 0–80 GPa for (MgO)m-(ZnO)n system ($n + m \leq 30$), and determined the compositions of the $Mg_xZn_{1-x}O$. To confirm this and to obtain the most accurate results, we then renewed our structure search of stoichiometric $Mg_mZn_nO_{m+n}$ with m and n values fixed by the USPEX code.

Total energy calculations. The structural optimizations, electronic structure, phonon dispersion, and energy calculations for selected structures are performed with CASTEP code[59]. The local density approximation (LDA-CAPZ)[52,53] approaches of exchange-correlation functional is employed. The norm-conserving pseudopotentials[60] with cutoff energy of 700 eV are used, and a k-mesh of $0.03 \times 2\pi$ Å^{-1} within the Monkhorst-Pack scheme for sample the Brillouin zone, which ensures the error bars of total energies are less than 1 meV/atom. The hybrid functional HSE06[54,55] implemented in the CASTEP code, together with norm-conserving pseudopotentials, and a cutoff energy of 600 eV, are used to calculate the band gaps of the stable structures at 10 GPa and 80 GPa.

1. Tsukazaki, A. *et al.* Repeated temperature modulation epitaxy for p-type doping and light-emitting diode based on ZnO. *Nat. Mater.* **4**, 42–46 (2005).
2. Belogorokhov, A. *et al.* Lattice vibrational properties of ZnMgO grown by pulsed laser deposition. *Appl. Phys. Lett.* **90**, 192110–192113 (2007).
3. Wu, C. *et al.* Characterization of $Mg_xZn_{1-x}O$ thin films grown on sapphire substrates by metalorganic chemical vapor deposition. *Thin Solid Films* **519**, 1966–1970 (2011).
4. Sans, J. A. & Segura, A. Optical properties and structural phase transitions in $Mg_xZn_{1-x}O$ under hydrostatic pressure. *High Pressure Res.* **24**, 119–127 (2004).
5. Wassner, T. A. *et al.* Optical properties and structural characteristics of ZnMgO grown by plasma assisted molecular beam epitaxy. *J. Appl. Phys.* **105**, 023505 (2009).
6. Ohtomo, A. *et al.* $Mg_xZn_{1-x}O$ as a II–VI widegap semiconductor alloy. *Appl. Phys. Lett.* **72**, 2466–2468 (1998).
7. Sharma, A. K. *et al.* Optical and structural properties of epitaxial $Mg_xZn_{1-x}O$ alloys. *Appl. Phys. Lett.* **75**, 3327–3329 (1999).
8. Choopun, S. *et al.* Realization of band gap above 5.0 eV in metastable cubic-phase $Mg_xZn_{1-x}O$ alloy films. *Appl. Phys. Lett.* **80**, 1529–1531 (2002).
9. Vashaei, Z. *et al.* Structural variation of cubic and hexagonal $Mg_xZn_{1-x}O$ layers grown on MgO(111)/c-sapphire. *J. Appl. Phys.* **98**, 054911 (2005).
10. Shan, F. K. Blueshift of near band edge emission in Mg doped ZnO thin films and aging. *J. Appl. Phys.* **95**, 4772–4776 (2004).
11. Bergman, L., Morrison, J. L., Chen, X.-B., Huso, J. & Hoeck, H. Ultraviolet photoluminescence and Raman properties of MgZnO nanopowders. *Appl. Phys. Lett.* **88**, 023103 (2006).

12. Huso, J. *et al*. Low temperature LO-phonon dynamics of MgZnO nanoalloys. *Appl. Phys. Lett.* **91**, 111906 (2007).
13. Huso, J. *et al*. Pressure response of the ultraviolet photoluminescence of ZnO and MgZnO nanocrystallites. *Appl. Phys. Lett.* **89**, 171909 (2006).
14. Hsu, H.-C., Wu, C.-Y., Cheng, H.-M. & Hsieh, W.-F. Band gap engineering and stimulated emission of ZnMgO nanowires. *Appl. Phys. Lett.* **89**, 013101 (2006).
15. Ghosh, M. & Raychaudhuri, A. K. Structural and optical properties of $Zn_{1-x}Mg_xO$ nanocrystals obtained by low temperature method. *J. Appl. Phys.* **100**, 034315 (2006).
16. Yang, W. *et al*. Ultraviolet photoconductive detector based on epitaxial $Mg_{0.34}Zn_{0.66}$ thin films. *Appl. Phys. Lett.* **78**, 2787–2789 (2001).
17. Jiang, D. Y. *et al*. Schottky Barrier Photodetectors Based on $Mg_{0.40}Zn_{0.60}O$ Thin Films. *Cryst. Growth Des.* **9**, 454–456 (2009).
18. Wang, L. K. *et al*. Single-crystalline cubic MgZnO films and their application in deep-ultraviolet optoelectronic devices. *Appl. Phys. Lett.* **95**, 131113 (2009).
19. Zheng, Q. *et al*. Dependence of structural and optoelectronic properties of sputtered $Mg_{0.50}Zn_{0.50}O$ films on substrate. *CrystEngComm* **15**, 2709–2713 (2013).
20. Wang, F. *et al*. Cross-like cubic $Zn_xMg_{1-x}O$ nanostructures. *J. Phys. D: Appl. Phys.* **46**, 055101 (2013).
21. Huso, J., Morrison, J. L., Bergman, L. & McCluskey, M. D. Anharmonic resonant Raman modes in $Mg_{0.2}Zn_{0.8}O$. *Phys. Rev. B* **87**, 125205 (2013).
22. Sanati, M., Hart, G. & Zunger, A. Ordering tendencies in octahedral MgO-ZnO alloys. *Phys. Rev. B* **68**, 155210 (2003).
23. Seko, A., Oba, F., Kuwabara, A. & Tanaka, I. Pressure-induced phase transition in ZnO and ZnO-MgO pseudobinary system: A first-principles lattice dynamics study. *Phys. Rev. B* **72**, 024107 (2005).
24. Liu, B., Seko, A. & Tanaka, I. Cluster expansion with controlled accuracy for the MgO/ZnO pseudobinary system via first-principles calculations. *Phys. Rev. B* **86**, 245202 (2012).
25. Aoumeur-Benkabou, F. Z., Ameri, M., Kadoun, A. & Benkabou, K. Theoretical Study on the Origins of the Gap Bowing in $Mg_xZn_{1-x}O$ Alloys. *Model. Numer. Simul. Mater. Sci.* **2**, 60–66 (2012).
26. Amrani, B., Ahmed, R. & El Haj Hassan, F. Structural, electronic and thermodynamic properties of wide band gap $Mg_xZn_{1-x}O$ alloy. *Comput. Mater. Sci.* **40**, 66–72 (2007).
27. Schleife, A. *et al*. Ab initio description of heterostructural alloys: Thermodynamic and structural properties of $Mg_xZn_{1-x}O$ and $Cd_xZn_{1-x}O$. *Phys. Rev. B* **81**, 245210 (2010).
28. Zhu, Y. *et al*. Electronic structure and phase stability of MgO, ZnO, CdO, and related ternary alloys. *Phys. Rev. B* **77**, 245209 (2008).
29. Kim, Y.-S., Lee, E.-C. & Chang, K. J. Stability of Wurtzite and Rocksalt $Mg_xZn_{1-x}O$ Alloys. *J. Korean Phys. Soc.* **39**, S92–S96 (2001).
30. Malashevich, A. & Vanderbilt, D. First-principles study of polarization in $Zn_{1-x}Mg_xO$. *Phys. Rev. B* **75**, 045106 (2007).
31. Zhang, Y. G., He, H. Y. & Pan, B. C. Structural phase transition and the related electronic and optical properties of MgZnO nanowires. *Eur. Phys. J. B* **80**, 395–400 (2011).
32. Zhang, X. D. *et al*. First-principles investigation of electronic and optical properties in wurtzite $Zn_{1-x}Mg_xO$. *Eur. Phys. J. B* **62**, 417–421 (2008).
33. Chen, X. & Kang, J. The structural properties of wurtzite and rocksalt $Mg_xZn_{1-x}O$. *Semicond. Sci. Technol.* **23**, 025008 (2008).
34. Chang, Y.-S. *et al*. Structural and optical properties of single crystal $Zn_{1-x}Mg_xO$ nanorods—Experimental and theoretical studies. *J. Appl. Phys.* **101**, 033502 (2007).
35. Shimada, K., Takahashi, N., Nakagawa, Y., Hiramatsu, T. & Kato, H. Nonlinear characteristics of structural properties and spontaneous polarization in wurtzite $Mg_xZn_{1-x}O$: A first-principles study. *Phys. Rev. B* **88**, 075203 (2013).
36. Lambrecht, W. R. L., Limpijumnong, S. & Segall, B. Theoretical study of ZnO and related $Mg_xZn_{1-x}O$ alloy band structures. *MIJ Internet J. Nitride Semicond. Res.* **4S1**, G6.8 (1999).
37. Thangavel, R., Rajagopalan, M. & Kumar, J. Theoretical investigations on $ZnCdO_2$ and $ZnMgO_2$ alloys: A first principle study. *Solid State Commun.* **137**, 507–511 (2006).
38. Thangavel, R., Prathiba, G., Naanci, B. A., Rajagopalan, M. & Kumar, J. First principle calculations of the ground state properties and structural phase transformation for ternary chalcogenide semiconductor under high pressure. *Comput. Mater. Sci.* **40**, 193–200 (2007).
39. Fan, X. F., Sun, H. D., Shen, Z. X., Kuo, J. L. & Lu, Y. M. A first-principle analysis on the phase stabilities, chemical bonds and band gaps of wurtzite structure $A_xZn_{1-x}O$ alloys (A = Ca, Cd, Mg). *J. Phys.: Condens. Matter* **20**, 235221 (2008).
40. Maznichenko, I. *et al*. Structural phase transitions and fundamental band gaps of $Mg_xZn_{1-x}O$ alloys from first principles. *Phys. Rev. B* **80**, 144101 (2009).
41. Wei, S.-H., Ferreira, L., Bernard, J. E. & Zunger, A. Electronic properties of random alloys: Special quasirandom structures. *Phys. Rev. B* **42**, 9622–9649 (1990).
42. Zunger, A., Wei, S.-H., Ferreira, L. & Bernard, J. E. Special quasirandom structures. *Phys. Rev. Lett.* **65**, 353–356 (1990).
43. Soven, P. Coherent-potential model of substitutional disordered alloys. *Phys. Rev.* **156**, 809–813 (1967).
44. Karzel, H. *et al*. Lattice dynamics and hyperfine interactions in ZnO and ZnSe at high external pressures. *Phys. Rev. B* **53**, 11425–11438 (1996).
45. Desgreniers, S. High-density phases of ZnO: Structural and compressive parameters. *Phys. Rev. B* **58**, 14102–14105 (1998).
46. Bates, C. H., White, W. B. & Roy, R. New high-pressure polymorph of zinc oxide. *Science* **137**, 993 (1962).
47. Duffy, T. S., Hemley, R. J. & Mao, H.-k. Equation of state and shear strength at multimegabar pressures: Magnesium oxide to 227 GPa. *Phys. Rev. Lett.* **74**, 1371–1374 (1995).
48. Park, W. I., Yi, G.-C. & Jang, H. M. Metalorganic vapor-phase epitaxial growth and photoluminescent properties of $Zn_{1-x}Mg_xO$($0 \leq x \leq 0.49$) thin films. *Appl. Phys. Lett.* **79**, 2022–2024 (2001).
49. Oganov, A. R. & Glass, C. W. Crystal structure prediction using ab initio evolutionary techniques: Principles and applications. *J. Chem. Phys.* **124**, 244704 (2006).
50. Glass, C. W., Oganov, A. R. & Hansen, N. USPEX—evolutionary crystal structure prediction. *Comput. Phys. Commun.* **175**, 713–720 (2006).
51. Jaffe, J. E., Snyder, J. A., Lin, Z. J. & Hess, A. C. LDA and GGA calculations for high-pressure phase transitions in ZnO and MgO. *Phys. Rev. B* **62**, 1660–1665 (2000).
52. Perdew, J. P. & Zunger, A. Self-interaction correction to density-functional approximations for many-electron systems. *Phys. Rev. B* **23**, 5048–5079 (1981).
53. Ceperley, D. M. Ground State of the Electron Gas by a Stochastic Method. *Phys. Rev. Lett.* **45**, 566–569 (1980).
54. Krukau, A. V., Vydrov, O. A., Izmaylov, A. F. & Scuseria, G. E. Influence of the exchange screening parameter on the performance of screened hybrid functionals. *J. Chem. Phys.* **125**, 224106 (2006).
55. Heyd, J., Scuseria, G. E. & Ernzerhof, M. Hybrid functionals based on a screened Coulomb potential. *J. Chem. Phys.* **118**, 8207–8215 (2003).
56. Chen, J., Shen, W. Z., Chen, N. B., Qiu, D. J. & Wu, H. Z. The study of composition non-uniformity in ternary $Mg_xZn_{1-x}O$ thin films. *J. Phys.: Condens. Matter* **15**, L475–L482 (2003).
57. Schleife, A., Rödl, C., Furthmüller, J. & Bechstedt, F. Electronic and optical properties of $Mg_xZn_{1-x}O$ and $Cd_xZn_{1-x}O$ fromab initiocalculations. *New J. Phys.* **13**, 085012 (2011).
58. Li, K. Y., Kang, C. Y. & Xue, D. F. Electronegativity calculation of bulk modulus and band gap of ternary ZnO-based alloys. *Mater. Res. Bull.* **47**, 2902–2905 (2012).
59. Segall, M. *et al*. First-principles simulation: ideas, illustrations and the CASTEP code. *J. Phys.: Condens. Matter* **14**, 2717–2744 (2002).
60. Lin, J. S., Qteish, A., Payne, M. C. & Heine, V. Optimized and transferable nonlocal separable ab initio pseudopotentials. *Phys. Rev. B* **47**, 4174–4180 (1993).

Acknowledgments

This work was supported by the National Basic Research Program of China (No. 2011CB808200), Program for Changjiang Scholars and Innovative Research Team in University (No. IRT1132), National Natural Science Foundation of China (Nos. 11074090, 51032001, 11104102, 10979001, 51025206, 11204100), National Found for Fostering Talents of basic Science (No. J1103202), and Specialized Research Fund for the Doctoral Program of Higher Education (20110061120007, 20120061120008). Part of calculations were performed in the High Performance Computing Center (HPCC) of Jilin University.

Author contributions

F.-B.T. and T.C. conceived the research. F.-B.T. carried out the calculations. F.-B.T., T.C., D.-F.D., D.L., C.-B.C., X.-J.S., Z.-L.Z., B.-B.L. analyzed the data. F.-B.T. and T.C. wrote the paper.

Additional information

Supplementary information accompanies this paper at http://www.nature.com/scientificreports

Competing financial interests: The authors declare no competing financial interests.

How to cite this article: Tian, F.B. *et al*. Miscibility and ordered structures of MgO-ZnO alloys under high pressure. *Sci. Rep.* **4**, 5759; DOI:10.1038/srep05759 (2014).